Balanced Cross-Kerr Coupling for Superconducting Qubit Readout

Alex A. Chapple,[1,*] Othmane Benhayoune-Khadraoui,[1,*] Simon Richer,[1] and Alexandre Blais[1,2]
[1]Institut Quantique and Département de Physique, Université de Sherbrooke, Sherbrooke, J1K 2R1 Quebec, Canada
[2]CIFAR, Toronto, Ontario M5G 1M1, Canada

(Received 3 April 2025; revised 29 October 2025; accepted 4 November 2025; published 19 December 2025)

Dispersive readout, the standard method for measuring superconducting qubits, is limited by multiphoton qubit-resonator processes arising even at moderate drive powers. These processes degrade performance, causing dispersive readout to lag behind single- and two-qubit gates in both speed and fidelity. In this Letter, we propose a novel readout method, termed *junction readout*. Junction readout leverages the nonperturbative cross-Kerr interaction resulting from coupling a qubit and a resonator via a Josephson junction. Furthermore, by adding a capacitive coupling in parallel to the junction, Purcell decay induced by the exchange coupling can be suppressed. We also show that junction readout is more robust against deleterious multiphoton processes, and offers greater flexibility for resonator frequency allocation. Crucially, junction readout achieves superior performance compared to dispersive readout while maintaining similar hardware overhead. Numerical simulations show that junction readout can achieve fidelity exceeding 99.99% in under 30 ns of integration time, making it a promising alternative for superconducting qubit readout with current hardware.

DOI: 10.1103/r4v5-wyyt

Introduction—Fast and high-fidelity qubit measurement is a cornerstone of quantum information processing and fault-tolerant quantum computing. For example, in quantum error correction (QEC) protocols, each round of QEC relies on rapid single-shot readout of ancilla qubits to detect errors. Recent breakthroughs achieving break-even performance in surface [1,2] and bosonic codes [3–5] have relied on dispersive readout, a standard tool for measuring superconducting qubits. This readout operates by introducing a qubit-state dependent shift in the resonator frequency, enabling qubit state inference without directly disturbing the qubit [6–8].

Despite the improvements in readout fidelity and integration times [9–13], dispersive readout still lags behind the performance of the best single- and two-qubit gates. Increasing the readout drive power to enhance fidelity and speed often leads to measurement-induced state transitions [14–21] which are detrimental to error correction protocols as they introduce correlated errors [22,23]. Resetting such states, which typically involve ∼5 to 10 photons [19], is challenging even with the use of leakage reduction techniques [24–27]. Thus, achieving fast, high-fidelity readout with low leakage rates remains an open problem.

To further complicate matters, state-of-the-art dispersive readout often requires a Purcell filter to prevent the qubit from decaying through the readout channel [28,29]. While effective, adding a Purcell filter increases the readout system's footprint, complicates calibration, and makes multiplexing more challenging. These challenges have spurred interest in intrinsically Purcell-protected qubits and readout methods as compact, scalable alternatives for next-generation quantum processors [30–34].

Here, we propose an approach to mediate a nonperturbative dispersive qubit-resonator interaction, enabling high-fidelity and fast measurement while suppressing the dominant channel contributing to Purcell decay. Even when accounting for reduced readout efficiency and finite qubit lifetime, our approach achieves an order-of-magnitude improvement over state-of-the-art readout systems with comparable hardware overhead.

Theory of junction readout—In circuit QED, the dispersive interaction $\sum_{i_t} \chi_{i_t} |i_t\rangle\langle i_t| \hat{a}^\dagger \hat{a}$, with $|i_t\rangle$ a bare transmon state and $\hat{a}$ the resonator's annihilation operator, is usually realized by capacitively coupling a qubit and a resonator that are widely detuned in frequency [8]. Here, we seek an alternative circuit that mediates this interaction, with the interaction strength $2\chi_z = \chi_{1_t} - \chi_{0_t}$ engineered to be nonperturbative (i.e., independent of the resonator frequency and not arising from a Schrieffer-Wolff-type frame transformation, in contrast to what one would obtain in the presence of a transverse coupling).

Alternative strategies for engineering a nonperturbative Kerr interaction have been explored [31–36]. In contrast to these approaches, which often involve complex circuit designs, rely on special symmetries, or encode qubits in spatially delocalized modes, our proposed circuits, shown in Fig. 1, offer a simpler solution with hardware overhead comparable to that of dispersive readout. In the circuit

*These authors contributed equally to this work.

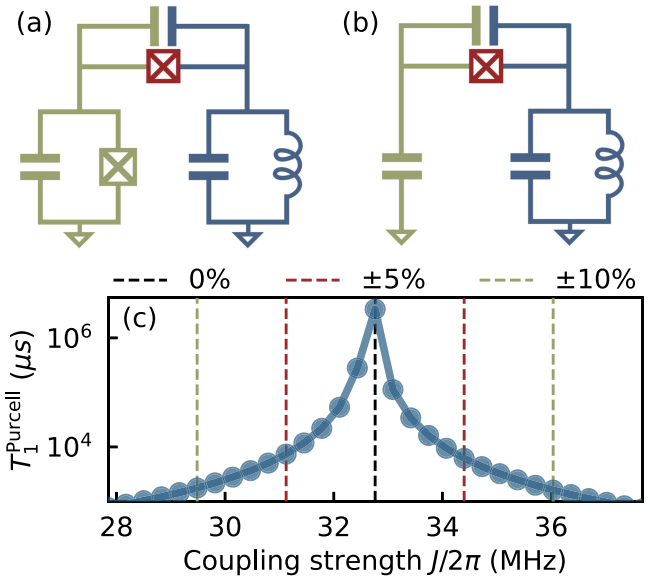

FIG. 1. Junction readout circuit (a) with and (b) without flux loop or low-frequency mode. A transmon (green) is coupled to the readout resonator (blue) through a Josephson junction (red) and a capacitor. Unlike in (a), in (b) the transmon nonlinearity is entirely inherited from the coupling junction, see Ref. [38]. (c) Jaynes–Cummings induced Purcell lifetime T_1^{Purcell} of the transmon for varying capacitive coupling strengths J. The black dashed line indicates where the cancellation condition of Eq. (3) is met. There, $J/2\pi \simeq 32.8$ MHz, corresponding to a coupling capacitance around 10 fF. The qubit and resonator frequencies are $\omega_q/2\pi = 5.672$ GHz and $\omega_r/2\pi = 9.375$ GHz, respectively, and the resonator decay rate is $\kappa/2\pi = 8$ MHz; see Sec. S2 of Ref. [38].

Fig. 1(a), the transmon (green) is coupled to a readout resonator (blue) through a Josephson junction in parallel with a capacitor whose role will be discussed below. The Hamiltonian of this circuit takes the form

$$\begin{aligned}\hat{H} &= 4E_C(\hat{n}_t - n_g)^2 - E_J\cos\hat{\varphi}_t + \omega_r\hat{a}^\dagger\hat{a} \\ &\quad - E_{J_c}\cos(\hat{\varphi}_t - \hat{\varphi}_r) + J\hat{n}_t\hat{n}_r \\ &\equiv \hat{H}_{\text{tr}} + \hat{H}_{\text{r}} + \hat{H}_{\text{int}},\end{aligned} \tag{1}$$

where the first (second) line corresponds to the transmon (resonator) Hamiltonian $\hat{H}_{\text{tr}}$ ($\hat{H}_{\text{r}}$) while the last line corresponds to the interaction Hamiltonian $\hat{H}_{\text{int}}$. Furthermore, $\hat{\varphi}_t$ and $\hat{n}_t$ are the transmon's phase and charge operators which satisfy the relation $[e^{i\hat{\varphi}_t}, \hat{n}_t] = -e^{i\hat{\varphi}_t}$, and E_J and E_C are its Josephson and charging energies, respectively. The resonator has frequency ω_r, and its phase operator is given by $\hat{\varphi}_r = \varphi_{\text{zpfr}}(\hat{a} + \hat{a}^\dagger)$ where $\varphi_{\text{zpfr}} = (2\pi/\Phi_0)\sqrt{\hbar Z_r/2}$ is the phase zero-point fluctuations. Furthermore, E_{J_c} is the Josephson energy of the coupling junction, and J is the capacitive coupling strength between the transmon and the resonator. The gate charge n_g is included explicitly, as it has been shown to affect the onset of measurement-induced state transitions [18,19,21,37]. As we show below, our proposed circuit ensures a high measurement critical photon number regardless of the value of the gate charge.

Setting $J = 0$ for the moment, the coupling Hamiltonian can be written in the form

$$\hat{H}_{\text{int}} = -E_{J_c}\cos\hat{\varphi}_t\cos\hat{\varphi}_r - E_{J_c}\sin\hat{\varphi}_t\sin\hat{\varphi}_r. \tag{2}$$

To second order in phase fluctuations, the cos-cos interaction of the first term leads to $\hat{\varphi}_t^2\hat{\varphi}_r^2$, thereby mediating a nonperturbative cross-Kerr coupling. As discussed in Ref. [39], this results in large measurement critical photon numbers and no Purcell decay. When supplemented with the appropriate resonator drive [39], this interaction emulates the longitudinal coupling discussed in Ref. [32], enabling fast and accurate discrimination of the pointer states. Here, we show that the circuit of Fig. 1 achieves the aforementioned benefits with a significantly simplified design. On the other hand, to first order in phase fluctuations, the sin-sin interaction term is an unwanted Jaynes-Cummings interaction that causes multiphoton resonances [15–19], thereby lowering the critical photon number; see Sec. S3A of Ref. [38]. A potential mitigation strategy is to substantially increase the qubit-resonator detuning—well beyond what it is used in standard dispersive readout—while simultaneously increasing the coupling to keep the dispersive shift fixed [40–42]. In practice, this places the qubit at a small fraction of the resonator frequency (e.g., $\omega_r/\omega_q \sim 10$) and thus relies on low-frequency qubits strongly coupled to high-frequency resonators, which introduces its own set of challenges.

Instead, here we propose to cancel this unwanted sin-sin term by introducing a parallel capacitance to the Josephson junction which mediates a charge-charge coupling $J\hat{n}_t\hat{n}_r$; see Fig. 1. The coupling strength J is specifically chosen to cancel the exchange (Jaynes-Cummings) coupling by setting the $0 \leftrightarrow 1$ matrix element of the interaction Hamiltonian to zero, as expressed by the condition

$$-E_{J_c}\langle 1_t, 0_r|\sin\hat{\varphi}_t\sin\hat{\varphi}_r|0_t, 1_r\rangle + J\langle 1_t, 0_r|\hat{n}_r\hat{n}_t|0_t, 1_r\rangle = 0, \tag{3}$$

where $|j_r\rangle$ denotes a bare resonator state. Intuitively, this condition—which we refer to as balanced cross-Kerr coupling—describes destructive interference between the current paths through the capacitor and the junction that mediate the exchange coupling between the qubit and readout modes; see also Ref. [43]. Importantly, since the cancellation condition involves only the computational subspace, the optimal coupling strength J is insensitive to fluctuations in the gate charge n_g. Moreover, as shown in Fig. 1(c), the Purcell decay—associated with the residual exchange coupling—remains minimal even when the condition Eq. (3) is not perfectly satisfied. For instance, with a

~10% imperfection in the junction or capacitor fabrication, the Purcell decay time T_1 remains on the order of ~1 ms for the chosen parameters [38], highlighting the robustness of this scheme to fabrication errors. In Sec. S8, we analyze the circuit shown in Fig. 1(b), which also realizes Eq. (1) but without involving a flux loop, along with other alternative circuit implementations.

Choice of readout parameters—We now turn to a discussion of the optimal choice of parameters. To achieve fast readout we aim for a large transmon-resonator cross-Kerr interaction. However, as is evident from Eq. (2), a nonperturbative cross-Kerr term (resulting from $\hat{\varphi}_t^2\hat{\varphi}_r^2$) is inherently accompanied by a nonperturbative self-Kerr nonlinearity on the resonator (resulting from $\hat{\varphi}_r^4$). Resonator self-Kerr can distort the coherent state in the resonator [44,45], potentially reducing readout fidelity by hindering the clear separation of pointer states and limiting the maximum photon population in the resonator. Moreover, this distortion renders the conventional linear measurement filter suboptimal for state assignment [46–48].

To achieve a large cross-Kerr interaction ($|\chi_z|/2\pi \sim$ 2–10 MHz) without compromising the linearity of the readout resonator, we optimize the resonator impedance Z_r. From Eq. (2), the leading contribution of the cross-Kerr strength is given by $\chi_z \simeq -\varphi_{\mathrm{zpfr}}^2 E_{Jc}\sqrt{2E_C/E_{J,\mathrm{total}}}/2$, with $E_{J,\mathrm{total}} = E_J + E_{Jc}$ which we keep constant. The self-Kerr nonlinearity of the resonator inherited from the coupling junction is approximately $K_r \simeq -E_{Jc}\varphi_{\mathrm{zpfr}}^4/2$. As a result, the cross-Kerr interaction decreases quadratically with the resonator phase zero-point fluctuations φ_{zpfr}, while the self-Kerr decreases quartically with φ_{zpfr}. Conversely, both χ_z and K_r increase linearly with respect to the coupling junction energy E_{Jc}. Since φ_{zpfr} depends on the resonator impedance Z_r, we optimize Z_r and E_{Jc} to achieve a large cross-Kerr coupling with minimal self-Kerr nonlinearity ($|K_r|/2\pi \lesssim 500$ kHz). Figures 2(a) and 2(b) show the cross-Kerr coupling strength χ_z and the resonator's self-Kerr K_r extracted from exact numerical diagonalization of Eq. (1) for a range of resonator impedances Z_r and coupling strengths E_{Jc}. For realistic circuit parameters, we are able to achieve a cross-Kerr coupling comparable to standard dispersive readout, typically ranging from 2 to 10 MHz. Furthermore, by slightly reducing the resonator impedance below 50 Ω—something that is easily achievable experimentally—the self-Kerr nonlinearity can be tuned to match, or in some cases even fall below, the typical values of 100 to 500 kHz observed in standard dispersive readout.

Interestingly, we also observe that, in junction readout, the dispersive shift shows minimal variation with increasing resonator photon numbers, in contrast to dispersive readout, where the dispersive shift decreases significantly. This difference arises from the nature of the qubit-resonator interaction which is different in the two schemes. Indeed, in junction readout, the cos-cos interaction leads to smaller higher-order

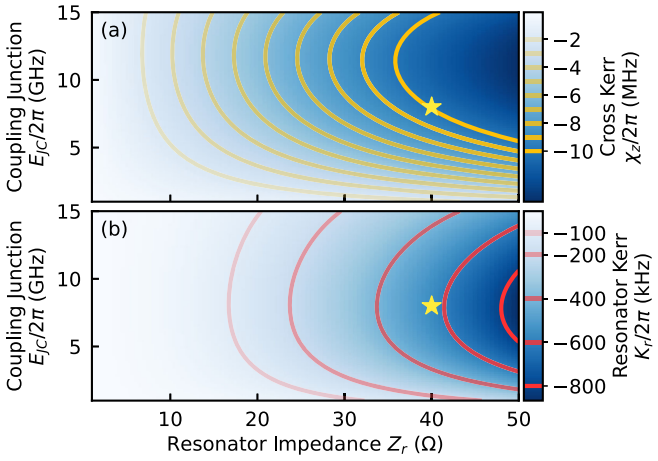

FIG. 2. (a) Cross-Kerr coupling χ_z and (b) resonator self-Kerr K_r between the transmon and the resonator for varying resonator impedance Z_r and coupling junction energy E_{Jc}. The contour lines indicate lines of constant (a) cross-Kerr ranging from −2 to −10 MHz and (b) self-Kerr ranging from −100 to −800 kHz. The star marks the parameter used in the readout simulations of Fig. 4.

corrections to the dispersive shift at large photon numbers compared to dispersive readout, enabling a faster readout as the cross-Kerr coupling remains large even when the resonator is populated, see Ref. [38] for further details.

The above analysis reveals that junction readout produces qubit-state-dependent frequency shifts similar to those of dispersive readout, suggesting comparable performance at first glance. In the following, we highlight the significant advantages offered by junction readout, demonstrating its superiority over dispersive readout in key aspects, namely its larger robustness against measurement-induced state transitions, as well as faster and higher fidelity measurements.

Suppressing ionization—The quantum nondemolition (QND) nature of dispersive readout is challenged by multiphoton processes arising due to accidental degeneracies between the qubit and the resonator [15]. This phenomenon, also referred to as ionization, occurs when two states of the transmon-resonator system become resonant as photons populate the resonator, leading to a sudden population transfer from the resonator to the transmon [15–19,21,49]. Because this process can typically involve highly excited states of the transmon which are charge sensitive, the resonator critical photon number n_{crit} at which these multiphoton processes occur can fluctuate widely with gate charge [18,19,21,37]. Note that n_{crit} here differs from the Jaynes-Cummings $n_{\mathrm{crit}}^{jc} = (\Delta/2g)^2$ which marks the breakdown of the dispersive approximation in dispersive readout [8]. We now show junction readout is far more robust against such multiphoton processes than dispersive readout.

To assess this robustness, we compute the critical photon numbers using branch analysis, a numerical tool predicting

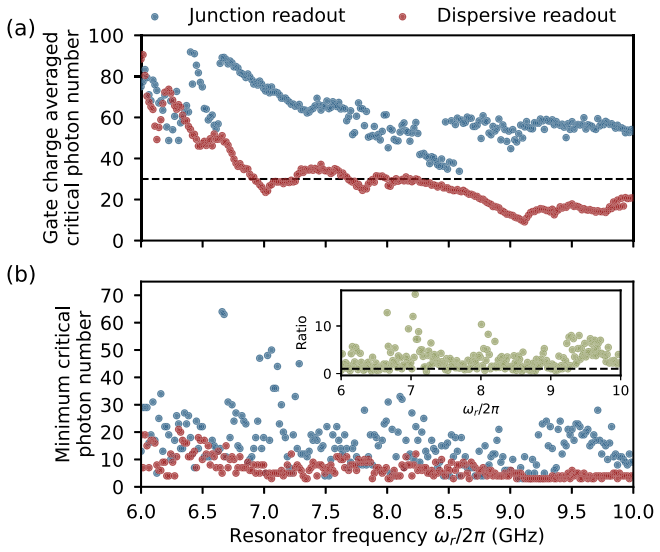

FIG. 3. (a) Critical photon number averaged over gate charge $n_g \in [0, 0.5]$ as a function of resonator frequency for junction readout (blue) and dispersive readout (red). In both cases, the dispersive shift is fixed at $|\chi_z|/2\pi \simeq 9$ MHz. Dashed horizontal line indicates $n_{\text{crit}} = 30$. (b) Minimum critical photon number over $n_g \in [0, 0.5]$. Inset: ratio of the minimum critical photon numbers between junction and dispersive readout. Dashed horizontal line indicates where the ratio is 1.

the onset of ionization and that has been shown to match experimental observations [21]; see Ref. [38] for further details in the context of junction readout. Figure 3(a) shows the critical photon number averaged over different realizations of the gate charge $n_g \in [0, 0.5]$, while panel (b) shows the minimum critical photon number across those realizations, for both junction readout (blue) and dispersive readout (red), over a wide range of resonator frequencies $\omega_r/2\pi \sim 6$–10 GHz. To ensure a fair comparison between both approaches, the dispersive shift is fixed to $|\chi_z|/2\pi \simeq 9$ MHz across all values of ω_r. For the dispersive readout, this requires adjusting the qubit-resonator coupling at all values of the resonator frequency [8]. We observe that junction readout consistently yields a higher average critical photon number than dispersive readout over nearly the entire range of resonator frequencies considered. Moreover, we show in Ref. [38] that for junction readout, there exists a broad region of resonator frequencies in which over 95% of gate charge realizations yield a critical photon number exceeding 30 [dashed horizontal line in Fig. 3(a)]. In contrast, no such frequency range exists for dispersive readout where a comparable fraction of realizations consistently surpass this threshold—see Ref. [38] for further details. Crucially, even in the worst-case scenario, the minimum critical photon number over realizations of the gate charge is larger for junction readout than for dispersive readout in most cases, as shown in Fig. 3(b).

The markedly higher ionization critical photon numbers observed in junction readout can be largely attributed to the cancellation condition of Eq. (3) Indeed, from perturbation theory, when the transmon ionizes to an excited state outside of the computational manifold, the transition occurs through virtual excitations, sequentially climbing the intermediate states between the initial state and the final ionized state [21]. The cancellation condition in Eq. (3), however, eliminates the matrix element responsible for the transition between the ground state and the first excited state, thereby preventing the initial step of leaving the computational subspace from the ground state. Additionally, while not exact, this cancellation approximately suppresses the matrix element responsible for transitions from the first to the second excited state, further reducing ionization when the qubit begins in its first excited state; see Sec. S3A for more details.

Finally, we further note that dispersive readout has less flexibility for frequency allocation as the dispersive shift depends on the resonator frequency, and often requires the readout resonator to be close in frequency to the qubit for a large dispersive shift. On the other hand, junction readout relies on a nonperturbative cross-Kerr interaction which does not depend on the resonator frequency, and thus offers greater flexibility for frequency allocation and potentially can alleviate frequency crowding issues for large-scale chips, whilst maintaining a large cross-Kerr for fast readout.

Readout performance—We have shown that junction readout can realize large cross-Kerr couplings together with small resonator self-Kerrs, higher critical photon numbers compared to dispersive readout across a wide range of resonator frequencies, and extended Purcell lifetimes. The ability to drive the resonator to large populations without encountering multiphoton resonances or significant leakage is crucial for achieving high-fidelity readout. In the following, we present numerical simulations of junction readout suggesting that fast, high-fidelity, and quantum nondemolition readout of transmons can be achieved with realistic parameters.

Our simulations are based on integrating the stochastic Schrödinger equation for heterodyne measurements of the resonator first assuming an ideal readout efficiency $\eta = 1$ [50]; see Ref. [38] for further details. Because they use the full Hamiltonian Eq. (1), these simulations account for the cross-Kerr, $|\chi_z|/2\pi \simeq 10$ MHz, but also the deleterious effect of the resonator self-Kerr, $|K_r|/2\pi \simeq 489$ kHz. A two-step measurement pulse leading to an average photon number of $\bar{n} \simeq 40$ photons is used, well below the critical photon number of $n_{\text{crit}} = 65$. Despite this short integration time, we find a large separation of the measurement result distribution for the two initial state using an optimal linear discriminator (black dashed line); see Fig. 4(b). The resulting assignment error vs the integration time t_m (full dark blue line) is reported in panel (c). For $\eta = 1$, a measurement fidelity of 99.99% is obtained in as short as $t_m = 20$ ns. Furthermore, we find a QNDness of 99.89%

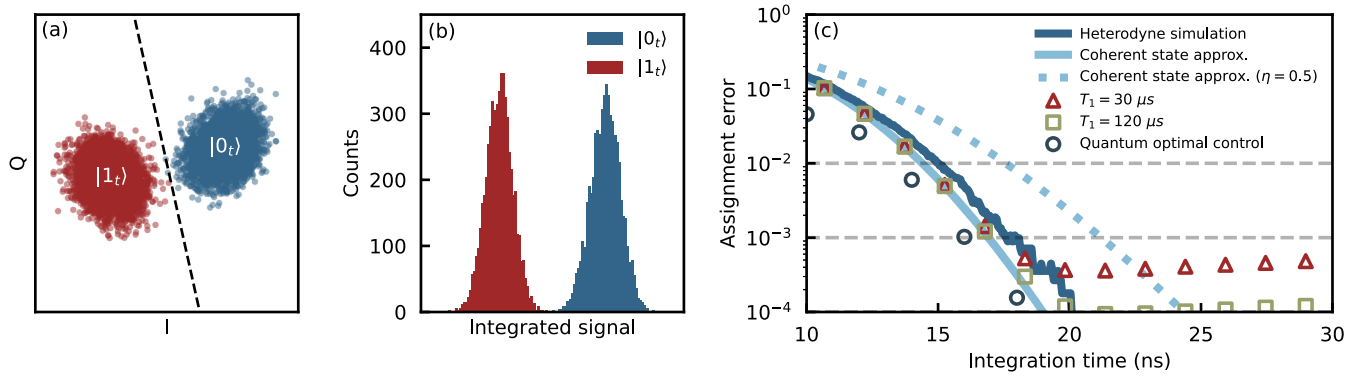

FIG. 4. (a) IQ plane of 11 200 single-shot heterodyne readout simulations of a transmon with junction readout. The black dashed line is the optimal discriminator of the two blobs corresponding to the qubit prepared in the ground (blue) or excited state (red). (b) Histogram of the integrated signal using an optimal discriminator. For both (a) and (b) the integrated time is $t_m \simeq 20$ ns. (c) Assignment error obtained from the stochastic heterodyne readout simulations compared to coherent state approximated assignment error. Using the coherent state approximated assignment error, we also show the assignment error for readout efficiency of $\eta = 0.5$ (where $0 \leq \eta \leq 1$) as well as when T_1 is 30 or 120 μs. Moreover, we show that quantum optimal control (QOC) further improves the readout fidelity. Here, the transmon charging energy is $E_C/2\pi = 300$ MHz with $E_{J,\mathrm{total}}/E_C = 50$ and gate charge $n_g = 0.0$. The resonator frequency is $\omega_r/2\pi = 9.375$ GHz, with resonator impedance $Z_r = 40\ \Omega$ and decay rate $\kappa/2\pi = 2|\chi_z| \simeq 20$ MHz. The junction coupling strength is $E_{J_c}/2\pi = 8$ GHz. This set of parameter results in a cross-Kerr of $|\chi_z|/2\pi \simeq 10$ MHz, and a critical photon number of $n_{\mathrm{crit}} = 65$.

and 99.71% for the ground and excited state, respectively [38].

Because of the small resonator self-Kerr, the distortion of the qubit-state-dependent resonator coherent states is relatively small; see Fig. 4(a). Under this condition, the resonator state can be approximated as coherent, allowing us to compare our numerical results with the analytical expression for the signal-to-noise ratio (SNR) and the assignment error [8,38,51]. The assignment error derived from this approximation (full light blue line) closely matches the full stochastic simulations. The small discrepancy is primarily due to the self-Kerr nonlinearity of the resonator. Given the good agreement between the numerical simulation and the coherent-state approximation, we use the latter to estimate the readout fidelity for finite transmon lifetime and nonideal readout efficiency, something which would be otherwise numerically challenging. First, for $T_1 = 30$ μs (red triangles), the readout fidelity comfortably exceeds 99.9% in $t_m \simeq 17$ ns. For a longer-lived transmon with $T_1 = 120$ μs (green squares), the fidelity surpasses 99.99% at $t_m \simeq 21$ ns. Second, assuming an infinite T_1 but a readout efficiency of $\eta = 0.5$ consistent with state-of-the-art experiments [10,13,20], we find a similar readout performance (dashed light blue line). Using quantum optimal control (QOC), the assignment error can be further reduced, enabling a readout fidelity of 99.99% within $t_m \simeq 18$ ns using realistic pulse shapes. With QOC, the same fidelity can also be achieved in 75 ns while including resonator reset [38]. We emphasize that these results are based on parameters readily achievable with current hardware. Even accounting for reduced efficiency and T_1 limitations, our results indicate that junction readout could achieve a fidelity exceeding 99.99% in under 30 ns of integration time, outperforming state-of-the-art readout experiments by an order of magnitude.

Conclusion—We have presented a circuit mediating a nonperturbative cross-Kerr coupling between a qubit and a readout resonator. The proposed junction readout method outperforms state-of-the-art dispersive readout by achieving higher critical photon numbers across a broad range of resonator frequencies and is less susceptible to the effect of gate charge. Notably, junction readout enhances the Purcell lifetime and has comparable hardware overhead to dispersive readout. Even when accounting for finite qubit lifetimes and reduced readout efficiency, this approach achieves a readout fidelity of 99.99% in under 30 ns of integration time. Junction readout overcomes many of the limitations posed by dispersive readout and can be implemented readily with only small modifications to current hardware. Junction readout could become a standard method for superconducting qubit measurement in next-generation quantum processors.

Note added—During the preparation of this Letter, we learned of similar work experimentally demonstrating Josephson junction-based readout of a transmon qubit [52]. In contrast to our approach, in that work the resonator nonlinearity induced by the coupling junction is large such that a high-power bifurcation readout is used.

Acknowledgments—The authors are grateful to Cristóbal Lledó for a critical reading of the manuscript, and to Peter Spring and Geneviève Gervais for insightful discussions.

This work was undertaken thanks in part to funding from the U.S. Army Research Office Grant No. W911NF-23-1-0101. Additional support is acknowledged from NSERC, the Canada First Research Excellence Fund, and the Ministère de l'Économie et de l'Innovation du Québec.

Data availability—The data that support the findings of this article are not publicly available upon publication because it is not technically feasible and/or the cost of preparing, depositing, and hosting the data would be prohibitive within the terms of this research project. The data are available from the authors upon reasonable request.

[1] Google Quantum AI, Suppressing quantum errors by scaling a surface code logical qubit, Nature (London) **614**, 676 (2023).
[2] Google Quantum AI, Quantum error correction below the surface code threshold, Nature (London) **638**, 920 (2025).
[3] N. Ofek, A. Petrenko, R. Heeres *et al.*, Extending the lifetime of a quantum bit with error correction in superconducting circuits, Nature (London) **536**, 441 (2016).
[4] V. V. Sivak, A. Eickbusch, B. Royer *et al.*, Real-time quantum error correction beyond break-even, Nature (London) **616**, 50 (2023).
[5] B. L. Brock, S. Singh, A. Eickbusch, V. V. Sivak, A. Z. Ding, L. Frunzio, S. M. Girvin, and M. H. Devoret, Quantum error correction of qudits beyond break-even, Nature (London) **641**, 612 (2025).
[6] A. Blais, R.-S. Huang, A. Wallraff, S. M. Girvin, and R. J. Schoelkopf, Cavity quantum electrodynamics for superconducting electrical circuits: An architecture for quantum computation, Phys. Rev. A **69**, 062320 (2004).
[7] A. Wallraff, D. I. Schuster, A. Blais, L. Frunzio, J. Majer, M. H. Devoret, S. M. Girvin, and R. J. Schoelkopf, Approaching unit visibility for control of a superconducting qubit with dispersive readout, Phys. Rev. Lett. **95**, 060501 (2005).
[8] A. Blais, A. L. Grimsmo, S. M. Girvin, and A. Wallraff, Circuit quantum electrodynamics, Rev. Mod. Phys. **93**, 025005 (2021).
[9] D. T. McClure, H. Paik, L. S. Bishop, M. Steffen, J. M. Chow, and J. M. Gambetta, Rapid driven reset of a qubit readout resonator, Phys. Rev. Appl. **5**, 011001 (2016).
[10] T. Walter, P. Kurpiers, S. Gasparinetti, P. Magnard, A. Potočnik, Y. Salathé, M. Pechal, M. Mondal, M. Oppliger, C. Eichler, and A. Wallraff, Rapid high-fidelity single-shot dispersive readout of superconducting qubits, Phys. Rev. Appl. **7**, 054020 (2017).
[11] Y. Sunada, S. Kono, J. Ilves, S. Tamate, T. Sugiyama, Y. Tabuchi, and Y. Nakamura, Fast readout and reset of a superconducting qubit coupled to a resonator with an intrinsic purcell filter, Phys. Rev. Appl. **17**, 044016 (2022).
[12] F. Swiadek, R. Shillito, P. Magnard, A. Remm, C. Hellings, N. Lacroix, Q. Ficheux, D. C. Zanuz, G. J. Norris, A. Blais, S. Krinner, and A. Wallraff, Enhancing dispersive readout of superconducting qubits through dynamic control of the dispersive shift: Experiment and theory, PRX Quantum **5**, 040326 (2024).
[13] P. A. Spring, L. Milanovic, Y. Sunada, S. Wang, A. F. van Loo, S. Tamate, and Y. Nakamura, Fast multiplexed superconducting-qubit readout with intrinsic purcell filtering using a multiconductor transmission line, PRX Quantum **6**, 020345 (2025).
[14] J. E. Johnson, C. Macklin, D. H. Slichter, R. Vijay, E. B. Weingarten, J. Clarke, and I. Siddiqi, Heralded state preparation in a superconducting qubit, Phys. Rev. Lett. **109**, 050506 (2012).
[15] D. Sank, Z. Chen, M. Khezri, J. Kelly, R. Barends, B. Campbell, Y. Chen, B. Chiaro, A. Dunsworth, A. Fowler, E. Jeffrey, E. Lucero, A. Megrant, J. Mutus, M. Neeley, C. Neill, P. J. J. O'Malley, C. Quintana, P. Roushan, A. Vainsencher, T. White, J. Wenner, A. N. Korotkov, and J. M. Martinis, Measurement-induced state transitions in a superconducting qubit: Beyond the rotating wave approximation, Phys. Rev. Lett. **117**, 190503 (2016).
[16] R. Lescanne, L. Verney, Q. Ficheux, M. H. Devoret, B. Huard, M. Mirrahimi, and Z. Leghtas, Escape of a driven quantum Josephson circuit into unconfined states, Phys. Rev. Appl. **11**, 014030 (2019).
[17] R. Shillito, A. Petrescu, J. Cohen, J. Beall, M. Hauru, M. Ganahl, A. G. Lewis, G. Vidal, and A. Blais, Dynamics of transmon ionization, Phys. Rev. Appl. **18**, 034031 (2022).
[18] J. Cohen, A. Petrescu, R. Shillito, and A. Blais, Reminiscence of classical chaos in driven transmons, PRX Quantum **4**, 020312 (2023).
[19] M. Khezri, A. Opremcak, Z. Chen, K. C. Miao, M. McEwen, A. Bengtsson, T. White, O. Naaman, D. Sank, A. N. Korotkov, Y. Chen, and V. Smelyanskiy, Measurement-induced state transitions in a superconducting qubit: Within the rotating-wave approximation, Phys. Rev. Appl. **20**, 054008 (2023).
[20] S. Hazra, W. Dai, T. Connolly, P. D. Kurilovich, Z. Wang, L. Frunzio, and M. H. Devoret, Benchmarking the readout of a superconducting qubit for repeated measurements, Phys. Rev. Lett. **134**, 100601 (2025).
[21] M. F. Dumas, B. Groleau-Paré, A. McDonald, M. H. Muñoz Arias, C. Lledó, B. D'Anjou, and A. Blais, Measurement-induced transmon ionization, Phys. Rev. X **14**, 041023 (2024).
[22] B. M. Varbanov, F. Battistel, B. M. Tarasinski, V. P. Ostroukh, T. E. O'Brien, L. DiCarlo, and B. M. Terhal, Leakage detection for a transmon-based surface code, npj Quantum Inf. **6**, 102 (2020).
[23] K. C. Miao, M. McEwen, J. Atalaya *et al.*, Overcoming leakage in quantum error correction, Nat. Phys. **19**, 1780 (2023).
[24] M. McEwen, D. Kafri, Z. Chen *et al.*, Removing leakage-induced correlated errors in superconducting quantum error correction, Nat. Commun. **12**, 1761 (2021).
[25] F. Battistel, B. Varbanov, and B. Terhal, Hardware-efficient leakage-reduction scheme for quantum error correction with superconducting transmon qubits, PRX Quantum **2**, 030314 (2021).
[26] J. F. Marques, H. Ali, B. M. Varbanov, M. Finkel, H. M. Veen, S. L. M. van der Meer, S. Valles-Sanclemente, N. Muthusubramanian, M. Beekman, N. Haider, B. M. Terhal, and L. DiCarlo, All-microwave leakage reduction units for

quantum error correction with superconducting transmon qubits, Phys. Rev. Lett. **130**, 250602 (2023).
[27] N. Lacroix, L. Hofele, A. Remm, O. Benhayoune-Khadraoui, A. McDonald, R. Shillito, S. Lazar, C. Hellings, F. m. c. Swiadek, D. Colao-Zanuz, A. Flasby, M. B. Panah, M. Kerschbaum, G. J. Norris, A. Blais, A. Wallraff, and S. Krinner, Fast flux-activated leakage reduction for superconducting quantum circuits, Phys. Rev. Lett. **134**, 120601 (2025).
[28] M. D. Reed, B. R. Johnson, A. A. Houck, L. DiCarlo, J. M. Chow, D. I. Schuster, L. Frunzio, and R. J. Schoelkopf, Fast reset and suppressing spontaneous emission of a superconducting qubit, Appl. Phys. Lett. **96**, 203110 (2010).
[29] E. Jeffrey, D. Sank, J. Y. Mutus, T. C. White, J. Kelly, R. Barends, Y. Chen, Z. Chen, B. Chiaro, A. Dunsworth, A. Megrant, P. J. J. O'Malley, C. Neill, P. Roushan, A. Vainsencher, J. Wenner, A. N. Cleland, and J. M. Martinis, Fast accurate state measurement with superconducting qubits, Phys. Rev. Lett. **112**, 190504 (2014).
[30] J. M. Gambetta, A. A. Houck, and A. Blais, Superconducting qubit with purcell protection and tunable coupling, Phys. Rev. Lett. **106**, 030502 (2011).
[31] I. Diniz, E. Dumur, O. Buisson, and A. Auffèves, Ultrafast quantum nondemolition measurements based on a diamond-shaped artificial atom, Phys. Rev. A **87**, 033837 (2013).
[32] N. Didier, J. Bourassa, and A. Blais, Fast quantum nondemolition readout by parametric modulation of longitudinal qubit-oscillator interaction, Phys. Rev. Lett. **115**, 203601 (2015).
[33] R. Dassonneville, T. Ramos, V. Milchakov, L. Planat, E. Dumur, F. Foroughi, J. Puertas, S. Leger, K. Bharadwaj, J. Delaforce, C. Naud, W. Hasch-Guichard, J. J. García-Ripoll, N. Roch, and O. Buisson, Fast high-fidelity quantum nondemolition qubit readout via a nonperturbative cross-Kerr coupling, Phys. Rev. X **10**, 011045 (2020).
[34] F. Pfeiffer, M. Werninghaus, C. Schweizer, N. Bruckmoser, L. Koch, N. J. Glaser, G. B. P. Huber, D. Bunch, F. X. Haslbeck, M. Knudsen, G. Krylov, K. Liegener, A. Marx, L. Richard, J. H. Romeiro, F. A. Roy, J. Schirk, C. Schneider, M. Singh, L. Södergren, I. Tsitsilin, F. Wallner, C. A. Riofrío, and S. Filipp, Efficient decoupling of a nonlinear qubit mode from its environment, Phys. Rev. X **14**, 041007 (2024).
[35] Y. Ye, K. Peng, M. Naghiloo, G. Cunningham, and K. P. O'Brien, Engineering purely nonlinear coupling between superconducting qubits using a quarton, Phys. Rev. Lett. **127**, 050502 (2021).
[36] Y. Ye, J. B. Kline, S. Chen, A. Yen, and K. P. O'Brien, Ultrafast superconducting qubit readout with the quarton coupler, Sci. Adv. **10**, eado9094 (2024).
[37] M. Malekakhlagh, W. Shanks, and H. Paik, Optimization of the resonator-induced phase gate for superconducting qubits, Phys. Rev. A **105**, 022607 (2022).
[38] See Supplemental Material at http://link.aps.org/supplemental/10.1103/r4v5-wyyt for more information, which includes Refs. [53–82].
[39] A. A. Chapple, A. McDonald, M. H. Muñoz-Arias, and A. Blais, Robustness of longitudinal transmon readout to ionization, Phys. Rev. Appl. **24**, 034026 (2025).
[40] P. D. Kurilovich, T. Connolly, C. G. L. Bøttcher, D. K. Weiss, S. Hazra, V. R. Joshi, A. Z. Ding, H. Nho, S. Diamond, V. D. Kurilovich, W. Dai, V. Fatemi, L. Frunzio, L. I. Glazman, and M. H. Devoret, High-frequency readout free from transmon multi-excitation resonances, arXiv:2501.09161.
[41] T. Connolly, P. D. Kurilovich, V. D. Kurilovich, C. G. L. Bøttcher, S. Hazra, W. Dai, A. Z. Ding, V. R. Joshi, H. Nho, S. Diamond, D. K. Weiss, V. Fatemi, L. Frunzio, L. I. Glazman, and M. H. Devoret, Full characterization of measurement-induced transitions of a superconducting qubit, arXiv:2506.05306.
[42] W. Dai, S. Hazra, D. K. Weiss, P. D. Kurilovich, T. Connolly, H. K. Babla, S. Singh, V. R. Joshi, A. Z. Ding, P. D. Parakh, J. Venkatraman, X. Xiao, L. Frunzio, and M. H. Devoret, Spectroscopy of drive-induced unwanted state transitions in superconducting circuits, arXiv:2506.24070.
[43] M. Kounalakis, C. Dickel, A. Bruno, N. K. Langford, and G. A. Steele, Tuneable hopping and nonlinear cross-Kerr interactions in a high-coherence superconducting circuit, npj Quantum Inf. **4**, 1 (2018).
[44] V. Sivak, N. Frattini, V. Joshi, A. Lingenfelter, S. Shankar, and M. Devoret, Kerr-free three-wave mixing in superconducting quantum circuits, Phys. Rev. Appl. **11**, 054060 (2019).
[45] S. Boutin, D. M. Toyli, A. V. Venkatramani, A. W. Eddins, I. Siddiqi, and A. Blais, Effect of higher-order nonlinearities on amplification and squeezing in Josephson parametric amplifiers, Phys. Rev. Appl. **8**, 054030 (2017).
[46] C. C. Bultink, B. Tarasinski, N. Haandbæk, S. Poletto, N. Haider, D. J. Michalak, A. Bruno, and L. DiCarlo, General method for extracting the quantum efficiency of dispersive qubit readout in circuit QED, Appl. Phys. Lett. **112**, 092601 (2018).
[47] J. Gambetta, W. A. Braff, A. Wallraff, S. M. Girvin, and R. J. Schoelkopf, Protocols for optimal readout of qubits using a continuous quantum nondemolition measurement, Phys. Rev. A **76**, 012325 (2007).
[48] B. D'Anjou and W. A. Coish, Optimal post-processing for a generic single-shot qubit readout, Phys. Rev. A **89**, 012313 (2014).
[49] X. Xiao, J. Venkatraman, R. G. Cortiñas, S. Chowdhury, and M. H. Devoret, Diagrammatic method to compute the effective Hamiltonian of a driven nonlinear oscillator, Phys. Rev. Appl. **24**, 044021 (2025).
[50] H. M. Wiseman and G. J. Milburn, Quantum theory of field-quadrature measurements, Phys. Rev. A **47**, 642 (1993).
[51] J. Gambetta, W. A. Braff, A. Wallraff, S. M. Girvin, and R. J. Schoelkopf, Protocols for optimal readout of qubits using a continuous quantum nondemolition measurement, Phys. Rev. A **76**, 012325 (2007).
[52] C. Wang, F.-M. Liu, H. Chen, Y.-F. Du, C. Ying, J.-W. Wang, Y.-H. Huo, C.-Z. Peng, X. Zhu, M.-C. Chen, C.-Y. Lu, and J.-W. Pan, Longitudinal and nonlinear coupling for high-fidelity readout of a superconducting qubit, Phys. Rev. Lett. **135**, 060803 (2025).
[53] M. Boissonneault, J. M. Gambetta, and A. Blais, Improved superconducting qubit readout by qubit-induced nonlinearities, Phys. Rev. Lett. **105**, 100504 (2010).

[54] H. P. Breuer and F. Petruccione, *The Theory of Open Quantum Systems* (Oxford University Press, New York, 2002).
[55] M. Boissonneault, J. M. Gambetta, and A. Blais, Nonlinear dispersive regime of cavity QED: The dressed dephasing model, Phys. Rev. A **77**, 060305 (2008).
[56] L. Labarca, O. Benhayoune-Khadraoui, A. Blais, and A. Parra-Rodriguez, Toolbox for nonreciprocal dispersive models in circuit quantum electrodynamics, Phys. Rev. Appl. **22**, 034038 (2024).
[57] D. Sank, M. Khezri, S. Isakov, and J. Atalaya, Balanced coupling in electromagnetic circuits, Phys. Rev. Appl. **23**, 024012 (2025).
[58] J. Gambetta, A. Blais, M. Boissonneault, A. A. Houck, D. I. Schuster, and S. M. Girvin, Quantum trajectory approach to circuit QED: Quantum jumps and the zeno effect, Phys. Rev. A **77**, 012112 (2008).
[59] J. Gambetta, A. Blais, D. I. Schuster, A. Wallraff, L. Frunzio, J. Majer, M. H. Devoret, S. M. Girvin, and R. J. Schoelkopf, Qubit-photon interactions in a cavity: Measurement-induced dephasing and number splitting, Phys. Rev. A **74**, 042318 (2006).
[60] D. I. Schuster, A. Wallraff, A. Blais, L. Frunzio, R.-S. Huang, J. Majer, S. M. Girvin, and R. J. Schoelkopf, Ac stark shift and dephasing of a superconducting qubit strongly coupled to a cavity field, Phys. Rev. Lett. **94**, 123602 (2005).
[61] M. Boissonneault, J. M. Gambetta, and A. Blais, Dispersive regime of circuit QED: Photon-dependent qubit dephasing and relaxation rates, Phys. Rev. A **79**, 013819 (2009).
[62] J. Johansson, P. Nation, and F. Nori, QuTiP: An open-source Python framework for the dynamics of open quantum systems, Comput. Phys. Commun. **183**, 1760 (2012).
[63] J. Johansson, P. Nation, and F. Nori, QuTiP 2: A Python framework for the dynamics of open quantum systems, Comput. Phys. Commun. **184**, 1234 (2013).
[64] R. Gautier, Élie Genois, and A. Blais, Optimal control in large open quantum systems: The case of transmon readout and reset, Phys. Rev. Lett. **134**, 070802 (2025).
[65] P. Guilmin, R. Gautier, A. Bocquet, É. Genois, and D. Weiss, Dynamiqs: An open-source Python library for GPU-accelerated and differentiable simulation of quantum systems, in preparation, (2025).
[66] R. T. Lange, evosax: JAX-based evolution strategies, arXiv:2212.04180.
[67] J. Rader, T. Lyons, and P. Kidger, Optimistix: Modular optimisation in JAX and Equinox, arXiv:2402.09983.
[68] This simplification also ensures a fair comparison with the grounded case since it maintains similar strong coupling between the transmon and the readout resonator. Alternatively, if $C_0 \simeq C_1$, the charge-charge coupling is reduced by a factor of 2, as expected from floating the qubit, and the cross-Kerr interaction is similarly reduced by a factor of 4 relative to the asymmetric case.
[69] S. Singh, G. Refael, A. Clerk, and E. Rosenfeld, Impact of Josephson junction array modes on fluxonium readout, PRX Quantum **6**, 040304 (2025).
[70] B. Hoyau, Transmon ionization in the presence of spectator qubits, in *APS Global Physics Summit, Anaheim, CA, March 2025*, (MAR-Q17 ID: 3106020, 2025).
[71] O. Benhayoune-Khadraoui, C. Lledó, and A. Blais, How the Kerr-CAT qubit dies-and how to rescue it, arXiv:2507.06160.
[72] P. Bertet, I. Chiorescu, G. Burkard, K. Semba, C. J. P. M. Harmans, D. P. DiVincenzo, and J. E. Mooij, Dephasing of a superconducting qubit induced by photon noise, Phys. Rev. Lett. **95**, 257002 (2005).
[73] A. A. Clerk and D. W. Utami, Using a qubit to measure photon-number statistics of a driven thermal oscillator, Phys. Rev. A **75**, 042302 (2007).
[74] A. P. Sears, A. Petrenko, G. Catelani, L. Sun, H. Paik, G. Kirchmair, L. Frunzio, L. I. Glazman, S. M. Girvin, and R. J. Schoelkopf, Photon shot noise dephasing in the strong-dispersive limit of circuit QED, Phys. Rev. B **86**, 180504 (2012).
[75] X. Ma *et al.*, Native approach to controlled-z gates in inductively coupled fluxonium qubits, Phys. Rev. Lett. **132**, 060602 (2024).
[76] A. Chakraborty, B. Bhandari, D. D. Briseño-Colunga, N. Stevenson, Z. Pedramrazi, C.-H. Liu, D. I. Santiago, I. Siddiqi, J. Dressel, and A. N. Jordan, Tunable superconducting quantum interference device coupler for fluxonium qubits, arXiv:2508.16907.
[77] D. M. Pozar, *Microwave Engineering*, 4th ed. (John Wiley & Sons, Hoboken, NJ, 2011).
[78] S. E. Nigg, H. Paik, B. Vlastakis, G. Kirchmair, S. Shankar, L. Frunzio, M. H. Devoret, R. J. Schoelkopf, and S. M. Girvin, Black-box superconducting circuit quantization, Phys. Rev. Lett. **108**, 240502 (2012).
[79] F. Solgun, D. W. Abraham, and D. P. DiVincenzo, Blackbox quantization of superconducting circuits using exact impedance synthesis, Phys. Rev. B **90**, 134504 (2014).
[80] F. Solgun and D. P. DiVincenzo, Multiport impedance quantization, Ann. Phys. (Amsterdam) **361**, 605 (2015).
[81] F. Solgun, D. P. DiVincenzo, and J. M. Gambetta, Simple impedance response formulas for the dispersive interaction rates in the effective Hamiltonians of low anharmonicity superconducting qubits, IEEE Trans. Microwave Theory Tech. **67**, 928 (2019).
[82] J. B. Kline, A. Yen, S. Chen, and K. P. O'Brien, The arm qubit: A superconducting qubit co-designed for coherence and coupling, arXiv:2506.05315.